

# School cohesion, speed, and efficiency are modulated by the swimmers flapping motion

Sina Heydari and Eva Kanso<sup>†</sup>

Aerospace and Mechanical Engineering, University of Southern California, Los Angeles,  
California 90089, USA

Fish schools are ubiquitous in marine life. Although flow interactions are thought to be beneficial for schooling, their exact effects on the speed, energetics, and stability of the group remain elusive. Recent experiments suggest that flow interactions stabilize in-tandem formations of heaving foils. Here, we propose a minimal approach based on the vortex sheet model that captures salient features of the flow interactions among flapping swimmers, and we study the free swimming of a pair of in-line swimmers driven with identical heaving or pitching motions. We find that, independent of the flapping mode, the follower passively stabilizes at discrete locations in the wake of the leader, consistent with the heaving foil experiments, but pitching swimmers exhibit tighter and more cohesive formations. Further, in comparison to swimming alone, pitching motions increase the energetic efficiency of the group while heaving motions result in a slight increase in the swimming speed. These results recapitulate that flow interactions provide a passive mechanism that promotes school cohesion, and provide novel insight into the role of the flapping mode in controlling the emergent properties of the school.

**Key words:** Pattern formation, hydrodynamics, swimming, vortex-sheet model, heaving and pitching swimmers

## 1. Introduction

Fish schools are ubiquitous in aquatic life, with half of the known fish species thought to exhibit schooling behavior during some phase of their life cycle (Shaw 1978). However, the role of the fluid medium as a mediator of the physical interactions between swimming fish remains unclear (Partridge & Pitcher 1979; Partridge 1982). Experimental evidence suggests that fish modify their motions and reduce muscular effort when swimming in vortex-laden flows (Liao *et al.* 2003). These findings support a long-standing but controversial hypothesis that schooling provides hydrodynamic benefits as fish move within the flows generated by others (Weihs 1973, 1975; Abrahams & Colgan 1985; Liao 2007). A direct assessment of this hypothesis in biological and physical models remains a challenge because of the complexity in resolving the hydrodynamics of unsteady swimming at high Reynolds numbers in single (Wolfgang *et al.* 1999; Triantafyllou *et al.* 2000; Borazjani 2008) and multiple interacting swimmers (Liao 2007; Gazzola *et al.* 2016; Verma *et al.* 2018). Simplifications based on crystalline school arrangements and ideal flow models indicate that fish within a planar formation, with diamond-shaped unit cell, benefit energetically from near-field interactions with the wakes of upstream neighbors (Weihs 1973), whereas far-field interactions serve to passively stabilize the

<sup>†</sup> Email address for correspondence: kanso@usc.edu

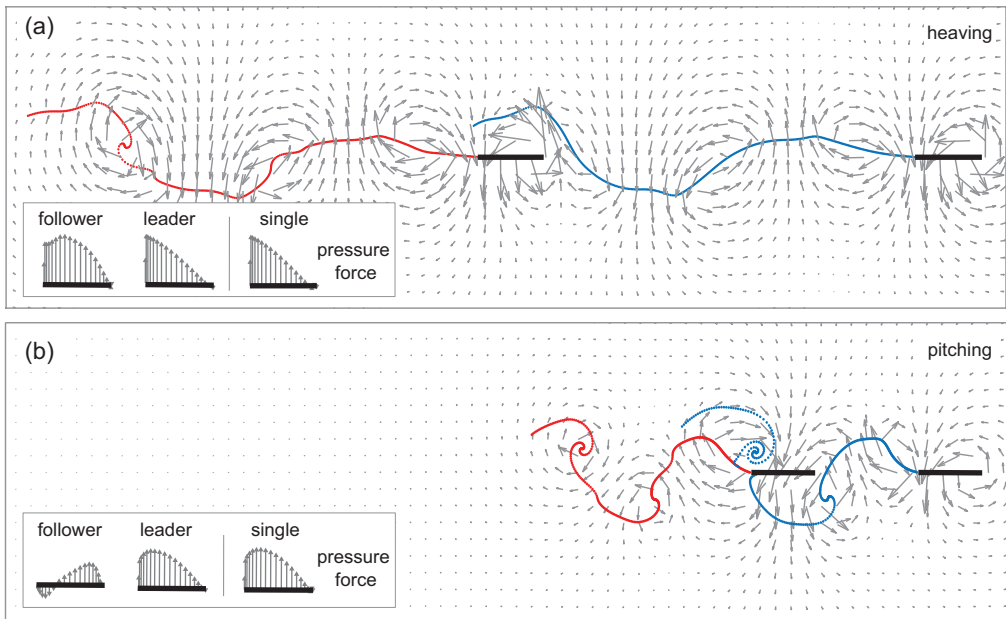


FIGURE 1. A pair of swimmers undergoing (a) heaving motions at amplitude  $A_h = 0.3$  and (b) pitching motions at amplitude  $A_p = 15^\circ$ . Snapshots of the velocity field (grey arrows) and free vortex sheet of the leader (blue) and follower (red) are taken after steady-state swimming is reached at a time instant where both swimmers are flapping downwards. Insets depict the pressure forces acting on each swimmer in the pairwise formation in comparison to a single swimmer undergoing the same prescribed motion.

formation (Tsang & Kanso 2013). These crystal lattice models do not capture that fish exhibit variable arrangements in field and laboratory experiments (Partridge & Pitcher 1979; Marras *et al.* 2015), and the broader question of how flow interactions benefit schooling remains unresolved.

Physical experiments on mechanically actuated foils found that, at the single swimmer level, flapping foils share with their biological counterparts many common aspects of the flows, forces, and energetics (Blondeaux *et al.* 2005; Lauder *et al.* 2011; Wen & Lauder 2013). A key similarity is the reverse von Kármán wake left by both flapping foils and fish (Taneda 1965; Triantafyllou & Triantafyllou 1993). More recently, flapping (heaving) foils were used for understanding multi-swimmer interactions (Becker *et al.* 2015; Ramananarivo *et al.* 2016; Newbolt *et al.* 2019). Heaving foils confined to in-line positions and freely swimming in tandem were found to assume one of several particular spacings. Flow interactions passively stabilize these ordered formations. Here, we investigate the speed, energetics, and stability of these planar formations using a mathematical model of self-propelling and interacting swimmers that flap by either heaving or pitching.

Existing mathematical models of flow interactions in fish schools vary in the degree of fidelity to the fluid dynamics and sensory-feedback control at the swimmer level. Ideal flow models – based on a dipolar far-field approximation (Tchieu *et al.* 2012) – with no feedback control have been used to assess the effect of passive flow interactions on the stability of pairwise (Kanso & Tsang 2014, 2015) and diamond lattice formations (Tsang & Kanso 2013) and the advantages of flapping out-of-phase (Kanso & Newton 2009). This far-field flow model coupled to visual feedback control, either in the form of behavioral rules (Filella *et al.* 2018) or learning algorithms (Gazzola *et al.* 2016), was

used to analyze the fish collective dynamics. Fish were shown to exhibit a novel collective turning mode and to swim faster thanks to the fluid (Filella *et al.* 2018). Near-field fish-wake interactions were also accounted for in ideal flow models with no feedback control, such as the vortex street model used by Weihs (1973) or the phenomenological model derived in Oza *et al.* (2019) to assess the efficiency of lattice formations. High-fidelity computational fluid dynamics coupled to reinforcement learning algorithms were recently implemented in pairwise interactions to optimize the flapping motion of the follower fish for harnessing the wake of the leader (Verma *et al.* 2018).

In this paper, we analyze pairwise interactions of heaving and pitching swimmers in the context of the vortex sheet model (see Figure 1). The vortex sheet model has been used extensively to analyze problems of fluid-structure interactions, including ring formation at the edge of a circular tube (Nitsche & Krasny 1994) and wakes of oscillating plates (Jones 2003; Sheng *et al.* 2012), falling cards (Jones 2005), flapping flexible flags (Alben & Shelley 2008; Alben 2009), swimming plates (Wu 1971) and hovering flyers (Huang *et al.* 2016, 2018). Here, we use the implementation of (Nitsche & Krasny 1994). We specifically focus on the effect of streamwise flow interactions on the swimming motion of heaving and pitching plates, and find that ordered formations emerge spontaneously via these interactions, independent of the flapping mode, consistent with the heaving foil experiments (Ramanananarivo *et al.* 2016). However, the flapping mode, heaving or pitching, affects the speed and energetics of these formations as well as their robustness to streamwise perturbations.

## 2. Problem formulation

A swimmer is modeled as a rigid plate of length  $2l$ , small thickness  $e \ll l$ , and homogenous density  $\rho$ , submerged in an unbounded, planar, fluid domain of density  $\rho_f$ . The swimmer's mass per unit depth is given by  $m = 2\rho e l$ . An inertial frame  $(\mathbf{e}_x, \mathbf{e}_y, \mathbf{e}_z)$  is introduced, such that  $(\mathbf{e}_x, \mathbf{e}_y)$  span the plane of motion. The vector  $\mathbf{x} \equiv (x, y)$  denotes the position of the geometric center of the swimmer in the  $(\mathbf{e}_x, \mathbf{e}_y)$  plane, and the angle  $\theta$  its orientation relative to the  $\mathbf{e}_x$ -direction (see Appendix A and Figure A)

The swimmer is free to move in the  $\mathbf{e}_x$ -direction under periodic heaving or pitching motions. Heaving consists of periodic lateral motions in the  $y$ -direction, of amplitude  $A_h$ , at fixed angle  $\theta = 0$ . Pitching refers to angular oscillations  $\theta$  of amplitude  $A_p$ , with zero lateral motion  $y = 0$  at the leading edge. The frequency of these heaving and pitching motions is denoted by  $f$ . Hereafter, we scale all parameter values using  $l$  as the characteristic length scale,  $1/f$  as the characteristic time scale, and  $\rho_f l^2$  as the characteristic mass per unit depth. Accordingly, velocities are scaled by  $lf$ , forces by  $\rho_f f^2 l^3$ , moments by  $\rho_f f^2 l^4$ , and power by  $\rho_f f^3 l^4$ .

In dimensionless form, the heaving and pitching motions are given by

$$\begin{aligned} \text{Heaving: } y(t) &= A_h \sin(2\pi t), & \theta(t) &= 0, \\ \text{Pitching: } \theta(t) &= A_p \sin(2\pi t), & y(t) &= 0. \end{aligned} \quad (2.1)$$

The equation of motion governing the free swimming  $x(t)$  is given by Newton's second law

$$m\ddot{x} = -F \sin \theta + S \cos \theta + D \cos \theta. \quad (2.2)$$

Here, the hydrodynamic forces acting on the swimmer consist of a leading edge suction force  $S$ , a pressure force  $F$  acting in the direction normal to the swimmer, and a skin drag force  $D$  acting tangentially to the swimmer. The drag force  $D$  is introduced to emulate the effect of fluid viscosity, while the hydrodynamic pressure force  $F$  is calculated in the

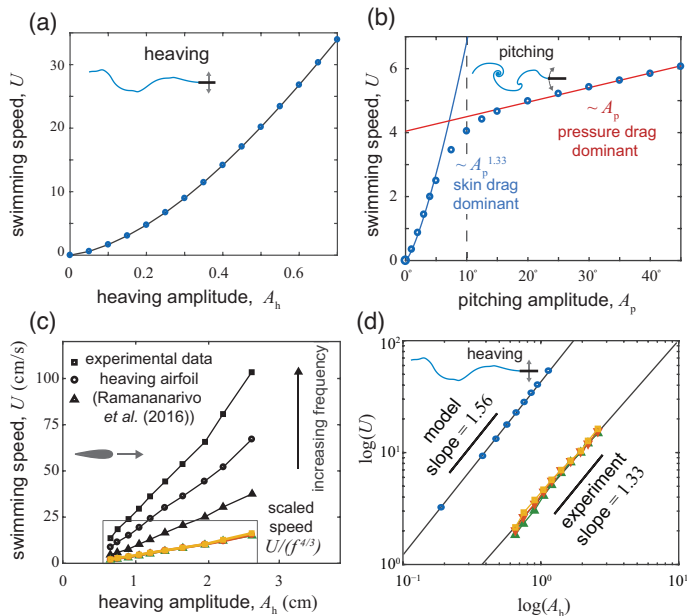


FIGURE 2. Swimming speed versus flapping amplitude for single swimmers. (a) Average swimming speed at steady state for a heaving swimmer. (b) Average swimming speed at steady state for a pitching swimmer. At small  $A_p$ , skin drag is dominant and the speed scales super-linearly with  $A_p$ . For  $A_p > 10^\circ$ , pressure drag is dominant and speed scales linearly with  $A_p$ . (c) Experimental data (black markers) of average swimming speed of a heaving foil (Ramanarivo *et al.* 2016, Figure 2); the data collapses when scaled by the heaving frequency  $f^{4/3}$  (yellow markers). (d) Comparing the swimming speed of our heaving swimmer model (blue circles) to the frequency-scaled experimental data shown in (a) on a log-log scale. Both model and experimental results scale super-linearly with heaving amplitude.

context of the inviscid vortex sheet model. A detailed description of the method and its numerical implementation can be found in Nitsche & Krasny (1994); Huang *et al.* (2018), and a brief overview is given in Appendix A. Detailed expressions of the fluid forces and moments acting on the swimmer are given in B.

To assess the swimming performance, we use four metrics: the period-averaged swimming speed  $U = \int_t^{t+1} \dot{x} dt$  at steady state, the thrust force  $T = S \cos \theta - F \sin \theta$ , the input power  $P$  required to maintain the prescribed heaving or pitching motions (see details in Appendix D), and the cost of transport defined as the input power  $P$  divided by the swimming speed  $U$ .

### 3. Single swimmers: numerical results and scaling analysis

We solve (2.2) in the case of a single swimmer and compute the period-average swimming speed at steady state. In Figure 2(a) and (b), we show the steady state speed for heaving and pitching swimmers, respectively, as a function of the flapping amplitude. In both cases, the speed increases monotonically, albeit that, when pitching, the increase scales differently at small amplitudes. To get insight into how the swimming speed  $U$  scales with the heaving and pitching amplitudes and frequency, it is instructive to use a simple scaling analysis.

At steady state, the sum of forces acting on the swimmer is zero on average. For heaving swimmers, the dominant forces are those due to the inertial added mass and

viscous skin drag. In dimensional form, the inertial force scales as  $\rho_f(2l)(A_h f)^2$ , where  $\rho_f(2l)A_h$  represents the mass of the laterally displaced fluid and  $A_h f^2$  its acceleration. Skin drag scales as  $\rho_f(2l)C_f U^2$ , where  $C_f \sim \sqrt{\mu/\rho_f(2l)U}$  is the drag coefficient based on adapting Blasius theory to this inviscid fluid model (see Appendix C and White (1979)). Balancing inertia and drag, we arrive at  $(A_h f)^2 \sim U^{3/2}$ , which leads to

$$\text{Heaving: } U \sim (A_h f)^{4/3}. \quad (3.1)$$

The swimming speed scales super-linearly with the heaving amplitude and frequency. We test this scaling law in light of the experimental results of (Ramanarivo *et al.* 2016, Figure 2). The black data points in Figure 2(c) represent the experimentally measured swimming speed as a function of heaving amplitude. The different marker shapes represent three different heaving frequencies used in the experiments ( $f = 1, 2, 3$ ). We scaled the data by the heaving frequency according to our derived scaling law in (3.1). The scaled data (colored markers) collapses on a single curve, indicating that our scaling analysis is sound. In Figure 2(d), we plot, using a log-log scale, the swimming speed obtained from our model in Figure 2(a) (blue dots) and experimental data (colored markers) versus the heaving amplitude. The slope of each line represents the power law that governs the relationship between the two quantities. In both the model and the experiment, the swimming speed depends super-linearly on the amplitude of heaving, however, the dependence is slightly stronger in the model.

The steady state speed of the pitching swimmer scales differently depending on the flapping amplitude because the dominant drag forces acting on the swimmer differ. At small pitching amplitude  $A_p$ , the swimmer is almost parallel to the swimming direction, hence skin drag is dominant leading to the same scaling law as in the heaving case. At large amplitude  $A_p$ , pressure drag is dominant; it is well known that pressure drag scales as  $U^2$ ; see, e.g., Moored & Quinn (2019). Balancing inertia and pressure drag, we arrive at  $U \sim A_p f$ . Put together, we have

$$\text{Pitching: } \begin{cases} \text{small } A_p : U \sim (A_h f)^{4/3}, \\ \text{large } A_p : U \sim A_p f. \end{cases} \quad (3.2)$$

These scaling laws fit remarkably well the numerical results in Figure 2(b).

#### 4. Pairwise formations: stability, speed, and energetics

We examine the steady state behavior of a pair of swimmers undergoing heaving and pitching motions while freely interacting via the fluid medium. In Figure 1, we show snapshots of the flow field (grey arrows) and free vortex sheets in the case when the leader (blue) and follower (red) are heaving at  $A_h = 0.3$  (Figure 1a) and pitching at  $A_p = 15^\circ$  (Figure 1b). The snapshots are taken after the pair has reached steady state swimming in the positive  $x$ -direction, and passively locked into a constant separation distance. At these flapping amplitudes, the heaving swimmers experience longer transience and swim faster, whereas the pitching swimmers rapidly lock into a tighter formation (see Supplemental Movie 1).

An analysis of the hydrodynamic pressure forces  $-F \sin \theta \mathbf{e}_x + F \cos \theta \mathbf{e}_y$ , where  $F$  is given in Appendix B, acting on each swimmer shows that compared to a single swimmer, the distribution on the leader remains relatively unchanged. However, the force distribution on the follower is affected by the wake of the leader, and the effect is more pronounced for pitching swimmers; see insets in Figure 1(a) and (b). Specifically in the pitching case, the follower experiences less resistance from the fluid, and a favorable

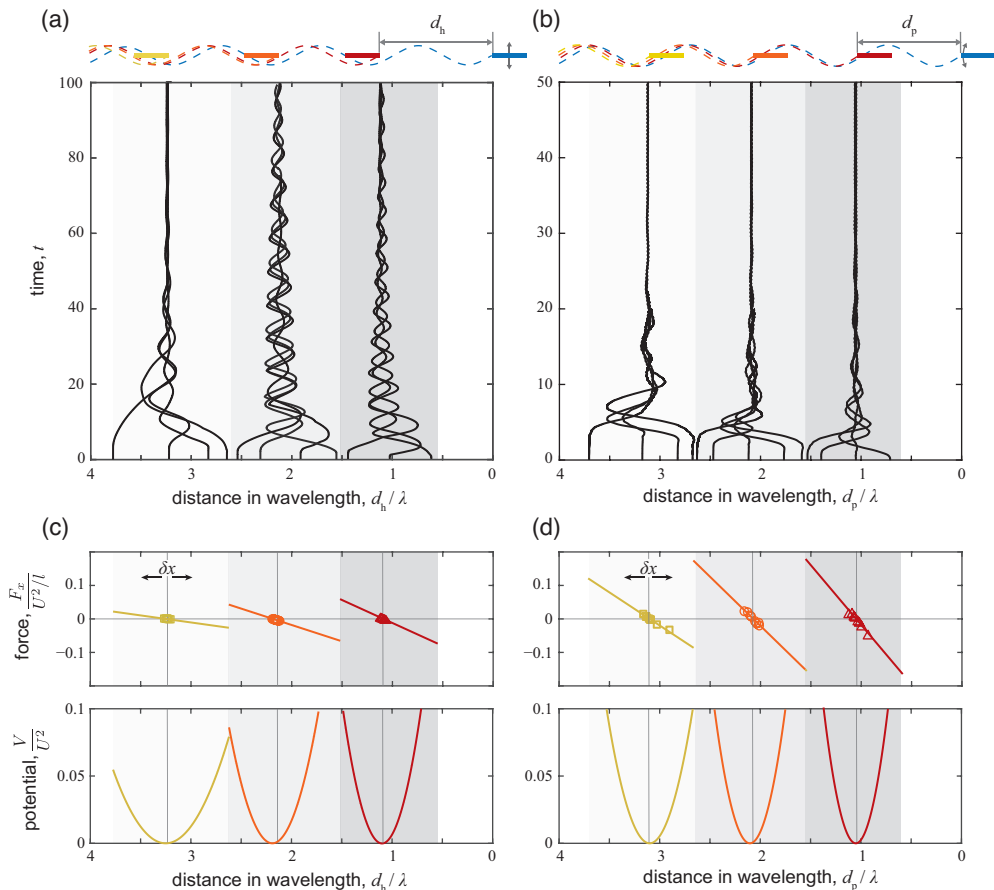


FIGURE 3. Emergence of passive stable formations in a pair of heaving swimmers ( $A_h = 0.3$ ) and of pitching swimmers ( $A_p = 15^\circ$ ). (a) For heaving swimmers, the follower stabilizes at one of many discrete positions behind the leader where the gap (tail-to-head) distance  $d_h$  is close to integer multiple of the wavelength  $\lambda = U/f$  of the leader motion. (b) For pitching swimmers, the follower stabilizes at locations such that the tail-to-tail distance  $d_p$  is close to integer multiples of  $\lambda$ . Basins of attraction of each the first three equilibria are depicted in gradually more faint shades of grey. (c) and (d) Linear stability analysis: we perturb the position of the follower about each of these equilibria and compute the total hydrodynamic force  $F_x$ . We simultaneously sample data from the change in  $F_x$  and perturbation strength  $\delta x$ , and plot  $\delta F_x$  versus  $\delta x$ . Clearly,  $\delta F_x$  acts as a restoring force. Taking the slope of  $\delta F_x$ , we construct the hydrodynamic potential  $V$  on the follower. The potential well is deepest at the first equilibrium where the hydrodynamic interactions are strongest.

force distribution (in the same direction of flapping) at the swimmer's tail. At the instant shown in Figure 1(b), the downward flow due to the vortex sheet created by the leader helps the follower in its downward pitching motion.

In Figure 3, we vary the initial separation distance between the two swimmers for the examples shown in Figure 1. We find that for both heaving and pitching, the follower tends to one of several discrete locations behind the leader at nearly digital values of  $d_h/\lambda$  and  $d_p/\lambda$ , respectively, where  $d_h$  is the tail-to-head distance,  $d_p$  the tail-to-tail distance, and  $\lambda = U/f$  the wavelength of the leader's swimming trajectory; see Figure 3(top). Depending on initial conditions, the leader and follower reach one of these separation distances and swim together in ordered formation. These findings are consistent with

experimental observations on heaving foils (Ramananarivo *et al.* 2016). The emergence of flow-mediated formation has not been previously reported for pitching swimmers.

We examine the nonlinear basins of attraction of these equilibria by varying the initial separation distance  $d_h$  and  $d_p$  between the two swimmers; The basin of attraction of each relative equilibrium is highlighted in a different shade of grey in Figure 3(a,b). The pitching swimmers converge more rapidly to the corresponding equilibria, indicating that these equilibria are stronger attractors in pitching than in heaving. Further, the wavelength  $\lambda = U/f$  is smaller in pitching, and so is the actual separation distance at equilibria ( $d_p < d_h$ ), indicating that pitching swimmers exhibit tighter formations.

To quantitatively assess the linear stability of these equilibria, we perturb the position of the follower about each equilibrium in the positive and negative  $x$ -direction with an initial perturbation of size  $\delta x/l = 0.5$  and we calculate the corresponding change in  $\delta x$  and change in the total hydrodynamic force  $\delta F_x = \delta(-F \sin \theta + S \cos \theta + D \cos \theta)$  acting on the follower in the  $x$ -direction. We scale the change in total force by  $U^2/l$  and the perturbation from equilibrium by  $d./\lambda$ , where  $d.$  is either  $d_h$  or  $d_p$ . We sample simultaneously the scaled change in total force  $\delta F_x$  and scaled perturbation strength  $\delta x$  and we plot the results in the first row of Figure 3(c,d). The results are depicted in red  $\triangle$  markers for the first stable position, and in orange  $\circ$  and yellow  $\square$  markers for the second and third positions, respectively. Straight line fit for each of these data sets results in straight lines with negative slopes, implying that, for each of these equilibrium positions, the hydrodynamic force acts as a restoring force  $\delta F_x = -K\delta x$  that keeps the formation stable. Here,  $K$  is obtained numerically from the straight line fit. The value of  $K$  depends monotonically on the equilibrium position of the follower, with highest value at the first equilibrium ( $d_h/\lambda \approx 1$  and  $d_p/\lambda \approx 1$ ). The first equilibrium is most stable because hydrodynamic interactions are strongest at closer distance. We write  $\delta F_x = -\partial V/\partial(\delta x)$ , where  $V = K(\delta x)^2/2$  is the hydrodynamic potential function around the equilibrium  $\delta x = 0$ . For both pitching and heaving, the formation is stable with weaker stability for larger inter-swimmer distance. In the pitching formation the potential well is deeper (by about 50%) for all equilibria, indicating faster convergence to the respective equilibrium.

We next evaluate the advantages of these formations in terms of the speed and energetics of the pair of swimmers in comparison to swimming alone. Figure 4 shows details of the time evolution at steady state of a single and pair of swimmers for the first relative equilibrium  $d_h/\lambda \approx 1$  and  $d_p/\lambda \approx 1$  shown in Figure 3, where hydrodynamic interactions are strongest. From top to bottom, we report the swimming speed, thrust force, input power and cost of transport versus time. Instantaneous values are shown in solid lines and period-average values in dashed lines. For the heaving motion, the average speed of the pair is about 10% higher than the speed of the single swimmer, consistent with experimental observations on heaving foils (Ramananarivo *et al.* 2016). However, the input power required to maintain these heaving motions in the presence of hydrodynamic interactions is also higher (about 30%). Consequently, the cost of transport of the heaving pair is about 20% higher than a single heaving swimmer. These results suggest that heaving swimmers can enhance their speed by swimming in a pair. However, this enhancement in swimming speed is achieved at an energetic cost.

For pitching swimmers, the speed of the formation is comparable to that of the single swimmer (about 2% slower). However, the follower's input power is significantly reduced (about 70% less than the single pitching swimmer). This reduction in input power is due to the hydrodynamic benefits highlighted in Figure 1(b). Correspondingly, the cost of transport of the pair of pitching swimmers drops by 30% compared to swimming alone.

Figure 5 explores the effect of the flapping amplitude on the period-average values of the swimming speed, thrust force, input power, and cost of transport, after the

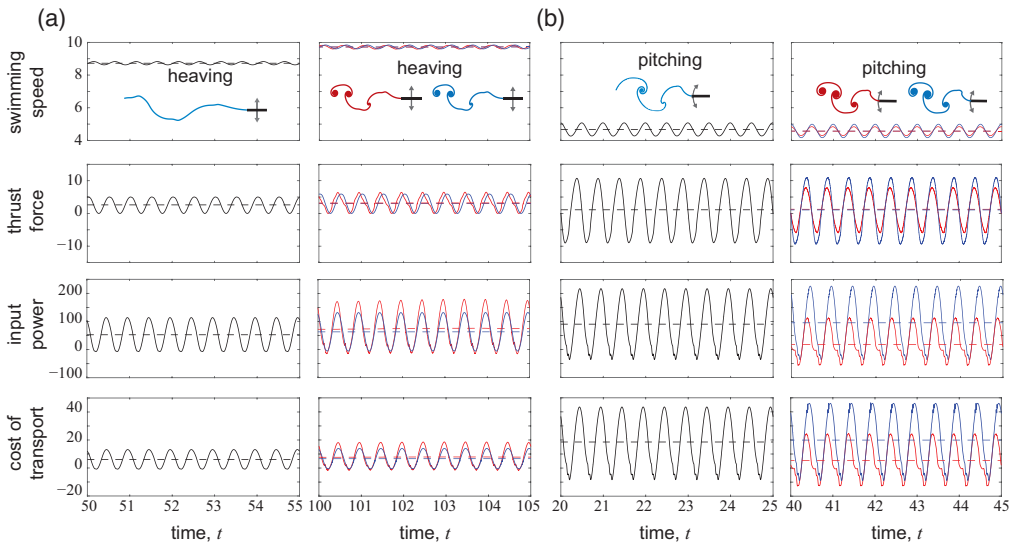


FIGURE 4. Instantaneous swimming performance (time-dependent speed, thrust, input power, and cost of transport versus time) for a single and pair of swimmers undergoing (a) heaving at  $A_h = 0.3$  and (b) pitching at  $A_p = 15^\circ$ , respectively. Results are shown after the swimmers have reached steady state. From top to bottom, the swimming speed, thrust force, input power and cost of transport are shown. Solid lines represent the instantaneous values and dashed lines represent time-period averages.

swimmers have reached steady state. Specifically, we examine the range  $A_h \in [0, 0.7]$  and  $A_p \in [0^\circ, 45^\circ]$  for single swimmers and  $A_h \in [0.3, 0.7]$  and  $A_p \in [10^\circ, 45^\circ]$  for pairs of swimmers, where small amplitudes are ignored to ensure that hydrodynamic interactions are sufficient for the spontaneous emergence of order formations. In pairwise interactions, we report all period-average values normalized by the corresponding values for a single swimmer.

When swimming alone, whether by heaving or pitching, an increase in the flapping amplitude monotonically increases the swimming speed, thrust, input power and cost of transport; see left columns of Figure 5(a) and (b). Here, the swimming speed versus flapping amplitude for single swimmers is a reproduction of the results in Figure 2(a,b).

Across all heaving amplitudes, the pairwise formation is about 5-10% faster than that of a single heaving swimmer. Both the leader and follower experience an increase in thrust compared to the single swimmer, but require more power to swim in formation compared to swimming alone, with extra power demand on the follower. The cost of transport of the heaving formation is thus slightly higher (around 15%) compared to swimming alone. Thus, heaving swimmers slightly enhance their swimming speed when in formation, albeit at a higher cost of transport.

The formation of pitching swimmers is about 5% slower than swimming alone for almost all flapping amplitudes. The leader experiences consistently lower thrust and the follower consistently higher thrust compared to swimming alone. However, while the power demand on the leader is comparable to the single swimmer, the power demand on the follower is significantly reduced for all amplitudes. Taken together, these results lead to slightly higher cost of transport for the leader and significantly lower cost of transport for the follower compared to swimming alone. Indeed, the cost of transport of the follower is a fraction of the single swimmer (around 25% at best), which in turn, causes the formation to save a significant amount of power (around 35% at best) compared to

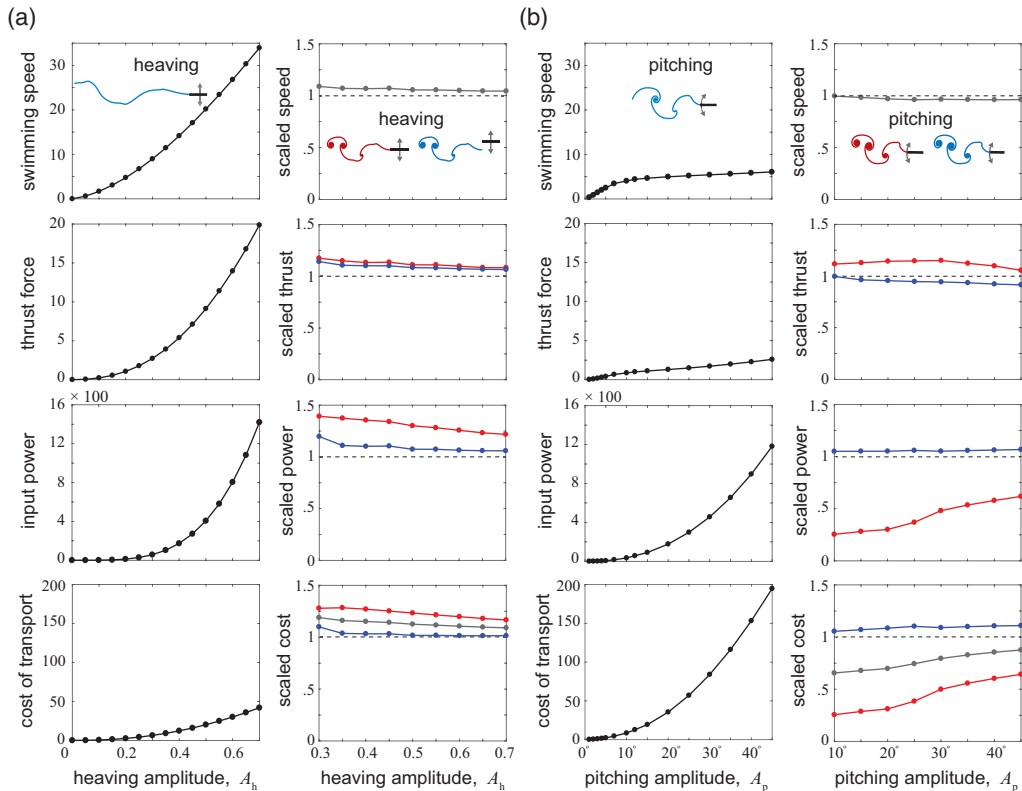


FIGURE 5. Swimming performance (average speed, thrust, input power, and cost of transport) versus flapping amplitude for a single and pair of swimmers undergoing (a) heaving and (b) pitching motions, respectively. From top to bottom, average values of the swimming speed, thrust force, input power and cost of transport. Left columns (black markers) in (a) and (b) show the results for single swimmers. For the pair of swimmers, all of the results are scaled by the corresponding quantity values for a single swimmer. The blue and red markers represent the results for the follower and leader, respectively. The grey markers are the school average.

swimming alone. These results imply that although the pairwise formation of pitching swimmers experiences no enhancement in swimming speed compared to swimming alone, it reduces the cost of transport by a significant amount.

## 5. Conclusion

We analyzed the locomotion dynamics of actively flapping swimmers interacting passively via the fluid medium in the context of the vortex sheet model. Within the two-swimmer model, we showed that hydrodynamic interactions lead to stable ordered formations, in which the follower falls into specific positions in the wake of the leader, and the pair travels together at the same speed. This well-ordered ‘schooling’ behavior occurs for both heaving and pitching swimmers. Group cohesion is tighter and more stable for pitching swimmers. In heaving, the school swims slightly faster compared to swimming alone, about 5-10% faster, albeit at a similar increases in cost of transport, especially for the follower (about 20% higher cost for the follower and 15% for the formation). When pitching, the school swims at a slightly (about 5%) lower speed but has significant

energetic benefits, with up to 35% reduction in cost of transport for the formation and up to 75% for the follower.

Our results are consistent with experimental findings of heaving foils (Becker *et al.* 2015; Ramananarivo *et al.* 2016; Newbolt *et al.* 2019), but go beyond these results in two major ways. Firstly, we provided a full assessment of the hydrodynamic benefits of schooling in terms of group stability, speed, and energetics. Experiments showed that heaving foils swim together in similar stable formations but the cost of heaving when in formation versus when swimming alone was not assessed in these studies. Secondly, we probed the effect of the flapping mode, heaving versus pitching, on the stability, speed, and energetic performance of the school, and we showed that the flapping mode affects the tightness and stability of the formation, as well as the cost of transport in school compared to swimming alone. Indeed, an alternative interpretation of our results is that they reveal how active changes in the flapping mode can be used to control, via hydrodynamic interactions, the school emergent properties, including the school speed, energetics, and cohesion. For example, to save energy or quickly overcome large perturbations, swimmers can adopt a pitching mode.

These findings could be instrumental for understanding the role of the fluid medium as a mediator of the physical interactions between swimming fish, and to assess the hydrodynamic benefits to fish schooling. Fish have more complex flapping motions than simple heaving and pitching (Ayancik *et al.* 2020; Van Buren *et al.* 2019; Lin *et al.* 2019), and the compliance of the fish body is believed to play an important role in the flapping efficiency and ability to extract energy from ambient flows (Beal *et al.* 2006; Lucas *et al.* 2014; Jusufi *et al.* 2017; Quinn *et al.* 2014). These considerations, as well as extensions to arrays of swimmers in-tandem and side-by-side, potentially flapping at different amplitudes and phases as in Newbolt *et al.* (2019), will be treated in future works.

**Acknowledgment.** The authors would like to thank Michael J. Shelley and Leif Ristroph for interesting conversations. This work is partially supported by the National Science Foundation grant CBET 15-12192, the Office of Naval Research grants 12707602 and N00014-17-1-2062, and the Army Research Office grant W911NF-16-1-0074.

## REFERENCES

- ABRAHAM, M. V. & COLGAN, P. W. 1985 Risk of predation, hydrodynamic efficiency and their influence on school structure. *Environmental Biology of Fishes* **13** (3), 195–202.
- ALBEN, S. 2009 Wake-mediated synchronization and drafting in coupled flags. *Journal of Fluid Mechanics* **641**, 489.
- ALBEN, S. & SHELLEY, M. J. 2008 Flapping states of a flag in an inviscid fluid: bistability and the transition to chaos. *Physical review letters* **100** (7), 074301.
- AYANCIK, F., FISH, F. E & MOORED, K. W. 2020 Three-dimensional scaling laws of cetacean propulsion characterize the hydrodynamic interplay of flukes' shape and kinematics. *Journal of the Royal Society Interface* **17** (163), 20190655.
- BEAL, D. N., HOVER, F. S., TRIANTAFYLLOU, M. S., LIAO, J. C. & LAUDER, G. V. 2006 Passive propulsion in vortex wakes. *Journal of Fluid Mechanics* **549**, 385.
- BECKER, A. D., MASOUD, H., NEWBOLT, J. W., SHELLEY, M. J. & RISTROPH, L. 2015 Hydrodynamic schooling of flapping swimmers. *Nature Communications* **6**, 8514.
- BLONDEAUX, P., FORNARELLI, F., GUGLIELMINI, L., TRIANTAFYLLOU, M. S. & VERZICCO, R. 2005 Numerical experiments on flapping foils mimicking fish-like locomotion. *Physics of Fluids* **17** (11), 113601.
- BORAZJANI, I. 2008 *Numerical simulations of fluid-structure interaction problems in biological flows*. University of Minnesota.
- ELDRIDGE, J. D. 2019 *Mathematical Modeling of Unsteady Inviscid Flows*. Springer.

- FANG, F. 2016 Hydrodynamic interactions between self-propelled flapping wings. PhD thesis, New York University.
- FILELLA, A., NADAL, F., SIRE, C., KANSO, E. & ELOY, C. 2018 Model of collective fish behavior with hydrodynamic interactions. *Physical review letters* **120** (19), 198101.
- GAZZOLA, M., TCHIEU, A. A., ALEXEEV, D., DE BRAUER, A. & KOUMOUTSAKOS, P. 2016 Learning to school in the presence of hydrodynamic interactions. *Journal of Fluid Mechanics* **789**, 726–749.
- HUANG, Y., NITSCHKE, M. & KANSO, E. 2016 Hovering in oscillatory flows. *Journal of Fluid Mechanics* **804**, 531–549.
- HUANG, Y., RISTROPH, L., LUHAR, M. & KANSO, E. 2018 Bistability in the rotational motion of rigid and flexible flyers. *Journal of Fluid Mechanics* **849**, 1043–1067.
- JONES, M. A. 2003 The separated flow of an inviscid fluid around a moving flat plate. *Journal of Fluid Mechanics* **496**, 405.
- JONES, M. A. & SHELLEY, M. J. 2005 Falling cards. *Journal of Fluid Mechanics* **540**, 393–425.
- JUSUFI, A., VOGT, D. M., WOOD, R. J. & LAUDER, G. V. 2017 Undulatory swimming performance and body stiffness modulation in a soft robotic fish-inspired physical model. *Soft robotics* **4** (3), 202–210.
- KANSO, E. & NEWTON, P. K. 2009 Passive locomotion via normal-mode coupling in a submerged spring-mass system. *Journal of Fluid Mechanics* **641**, 205.
- KANSO, E. & TSANG, A. C. H. 2014 Dipole models of self-propelled bodies. *Fluid Dynamics Research* **46** (6), 061407.
- KANSO, E. & TSANG, A. C. H. 2015 Pursuit and synchronization in hydrodynamic dipoles. *Journal of Nonlinear Science* **25**(5), 1141.
- LAUDER, G. V., LIM, J., SHELTON, R., WITT, C., ANDERSON, E. & TANGORRA, J. L. 2011 Robotic models for studying undulatory locomotion in fishes. *Marine Technology Society Journal* **45** (4), 41–55.
- LIAO, J. C. 2007 A review of fish swimming mechanics and behaviour in altered flows. *Philosophical Transactions of the Royal Society B: Biological Sciences* **362** (1487), 1973–1993.
- LIAO, J. C., BEAL, D. N., LAUDER, G. V. & TRIANTAFYLLOU, M. S. 2003 Fish exploiting vortices decrease muscle activity. *Science* **302** (5650), 1566–1569.
- LIN, X., WU, J. & ZHANG, T. 2019 Performance investigation of a self-propelled foil with combined oscillating motion in stationary fluid. *Ocean Engineering* **175**, 33–49.
- LUCAS, K. N., JOHNSON, N., BEAULIEU, W. T., CATHCART, E., TIRRELL, G., COLIN, S. P., GEMMELL, B. J., DABIRI, J. O. & COSTELLO, J. H. 2014 Bending rules for animal propulsion. *Nature communications* **5** (1), 1–7.
- MARRAS, S., KILLEN, S. S., LINDSTRÖM, J., MCKENZIE, D. J., STEFFENSEN, J. F. & DOMENICI, P. 2015 Fish swimming in schools save energy regardless of their spatial position. *Behavioral ecology and sociobiology* **69** (2), 219–226.
- MOORED, K. W. & QUINN, D. B. 2019 Inviscid scaling laws of a self-propelled pitching airfoil. *AIAA Journal* **57** (9), 3686–3700.
- NEWBOLT, J. W., ZHANG, J. & RISTROPH, L. 2019 Flow interactions between uncoordinated flapping swimmers give rise to group cohesion. *Proceedings of the National Academy of Sciences* **116**, 201816098.
- NITSCHKE, M. & KRASNY, R. 1994 A numerical study of vortex ring formation at the edge of a circular tube. *Journal of Fluid Mechanics* **276**, 139–161.
- OZA, A. U., RISTROPH, L. & SHELLEY, M. J. 2019 Lattices of hydrodynamically interacting flapping swimmers. *Physical Review X* **9** (4), 041024.
- PARTRIDGE, B. L. 1982 The structure and function of fish schools. *Scientific american* **246** (6), 114–123.
- PARTRIDGE, B. L. & PITCHER, T. J. 1979 Evidence against a hydrodynamic function for fish schools. *Nature* **279** (5712), 418–419.
- QUINN, D. B., LAUDER, G. V. & SMITS, A. J. 2014 Scaling the propulsive performance of heaving flexible panels. *Journal of fluid mechanics* **738**, 250.
- RAMANANARIVO, S., FANG, F., OZA, A., ZHANG, J. & RISTROPH, L. 2016 Flow interactions lead to orderly formations of flapping wings in forward flight. *Phys. Rev. Fluids* **1**, 071201.

- SAFFMAN, P. G. 1992 *Vortex dynamics*. Cambridge university press.
- SHAW, E. 1978 Schooling fishes: the school, a truly egalitarian form of organization in which all members of the group are alike in influence, offers substantial benefits to its participants. *American Scientist* **66** (2), 166–175.
- SHENG, J. X., YSASI, A., KOLOMENSKIY, D., KANSO, E., NITSCHKE, M. & SCHNEIDER, K. 2012 Simulating vortex wakes of flapping plates. In *Natural locomotion in fluids and on surfaces*, pp. 255–262. Springer.
- TANEDA, S. 1965 Experimental investigation of vortex streets. *Journal of the Physical Society of Japan* **20** (9), 1714–1721.
- TCHIEU, A. A., KANSO, E. & NEWTON, P. K. 2012 The finite-dipole dynamical system. *Proceedings of the Royal Society A: Mathematical, Physical and Engineering Sciences* **468** (2146), 3006–3026.
- TRIAANTAFYLLOU, G. S. & TRIANTAFYLLOU, M. S. 1993 Reverse kármán streets in the wake of flapping foils for application in fish propulsion. In *Bluff-Body Wakes, Dynamics and Instabilities*, pp. 11–14. Springer.
- TRIAANTAFYLLOU, M. S., TRIANTAFYLLOU, G. S. & YUE, D. K. 2000 Hydrodynamics of fishlike swimming. *Annual review of fluid mechanics* **32** (1), 33–53.
- TSANG, A. C. H. & KANSO, E. 2013 Dipole interactions in doubly periodic domains. *Journal of Nonlinear Science* **23** (6), 971–991.
- VAN BUREN, T., FLORYAN, D. & SMITS, A. J. 2019 Scaling and performance of simultaneously heaving and pitching foils. *AIAA Journal* **57** (9), 3666–3677.
- VERMA, S., NOVATI, G. & KOUMOUTSAKOS, P. 2018 Efficient collective swimming by harnessing vortices through deep reinforcement learning. *Proceedings of the National Academy of Sciences* **115** (23), 5849–5854.
- WEIHS, D. 1973 Hydromechanics of fish schooling. *Nature* **241**, 241290a0.
- WEIHS, D. 1975 Some hydrodynamical aspects of fish schooling. In *Swimming and flying in nature*, pp. 703–718. Springer.
- WEN, L. & LAUDER, G. 2013 Understanding undulatory locomotion in fishes using an inertia-compensated flapping foil robotic device. *Bioinspiration & biomimetics* **8** (4), 046013.
- WHITE, F. M. 1979 *Fluid mechanics*. Tata McGraw-Hill Education.
- WOLFGANG, M. J., ANDERSON, J. M., GROSENBAUGH, M. A., YUE, D. K. & TRIANTAFYLLOU, M. S. 1999 Near-body flow dynamics in swimming fish. *Journal of Experimental Biology* **202** (17), 2303–2327.
- WU, T. 1971 Hydromechanics of swimming propulsion. part 1. swimming of a two-dimensional flexible plate at variable forward speeds in an inviscid fluid. *Journal of Fluid Mechanics* **46** (2), 337–355.

## Appendix A. Vortex sheet model

The coupled fluid-structure interaction between the swimming plate and the surrounding fluid is simulated using an inviscid vortex sheet model. In viscous fluids, boundary layer vorticity is formed along the sides of the swimmer, and it is swept away at the swimmer’s tail to form a shear layer that rolls up into vortices. In the vortex sheet model, the swimmer is approximated by a bound vortex sheet, denoted by  $l_b$ , whose strength ensures that no fluid flows through the rigid plate, and the separated shear layer is approximated by a free regularized vortex sheet  $l_w$  at the trailing edge of the swimmer. The total shed circulation  $\Gamma$  in the vortex sheet is determined so as to satisfy the Kutta condition at the trailing edge, which is given in terms of the tangential velocity components above and below the bound sheet and ensures that the pressure jump across the sheet vanishes at the trailing edge.

To express these concepts mathematically, it is convenient to use the complex notation  $z = x + iy$ , where  $i = \sqrt{-1}$  and  $(x, y)$  denote the components of an arbitrary point in the plane. The bound vortex sheet  $l_b$  is described by its position  $z_b(s, t)$  and strength  $\gamma(s, t)$ , where  $s \in [-l, l]$  denotes the arc length along the sheet  $l_b$ . The separated sheet

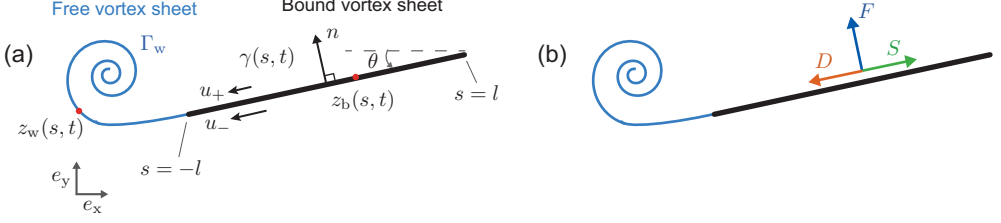


FIGURE 6. (a) Schematic of the vortex sheet model for a two-dimensional flapping swimmer. (b) Depiction of the different hydrodynamic forces acting on the swimmer.

$l_w$  is described by its position  $z_w(\Gamma, t)$ ,  $\Gamma \in [0, \Gamma_w]$  where  $\Gamma$  is the Lagrangian circulation around the portion of the separated sheet between its free end in the spiral center and the point  $z_w(\Gamma, t)$ . The parameter  $\Gamma$  defines the vortex sheet strength  $\gamma = d\Gamma/ds$ .

By linearity of the problem, the complex velocity  $w(z, t) = u(z, t) - iv(z, t)$  is a superposition of the contributions due to the bound and free vortex sheets

$$w(z, t) = w_b(z, t) + w_w(z, t). \quad (\text{A } 1)$$

In practice, the free sheet  $l_w$  is regularized using the vortex blob method to prevent the growth of the Kelvin-Helmholtz instability. The bound sheet  $l_b$  is not regularized in order to preserve the invertibility of the map between the sheet strength and the normal velocity along the sheet. The velocity components  $w_b(z, t)$  and  $w_w(z, t)$  induced by the bound and free vortex sheets, respectively, are given by

$$w_b(z, t) = \int_{-l}^l K_o(z - z_b(s, t)) \gamma(s, t) ds, \quad w_w(z, t) = \int_0^{\Gamma_w} K_\delta(z - z_w(\Gamma, t)) d\Gamma, \quad (\text{A } 2)$$

where  $K_\delta$  is the vortex blob kernel, with regularization parameter  $\delta$ ,

$$K_\delta(z) = \frac{1}{2\pi i} \frac{\bar{z}}{|z|^2 + \delta^2}, \quad \bar{z} = x - iy \quad (\text{A } 3)$$

If  $z$  is a point on the bound sheet for which  $\delta = 0$ ,  $w_b$  is to be computed in the principal value sense.

The position of the bound vortex sheet  $z_b$  is determined from the plate's flapping  $(y(t), \theta(t))$  and swimming  $x(t)$  motions. The corresponding sheet strength  $\gamma(s, t)$  is determined by imposing the no penetration boundary condition on the plate, together with conservation of total circulation. Let  $n(s, t) = -\sin \theta + i \cos \theta$  be the upward normal to the plate, the no penetration boundary condition is given by

$$\text{Re}[wn]_{z_b} = \text{Re}[w_{\text{swimmer}}n], \quad (\text{A } 4)$$

where

$$w_{\text{swimmer}} = \dot{x} - i\dot{y} - i\dot{\theta}[\bar{z}_b - (x - iy)]. \quad (\text{A } 5)$$

Conservation of the fluid circulation implies that  $\int_{l_b} \gamma(s, t) ds + \Gamma_w(t) = 0$ .

The circulation parameter  $\Gamma$  along the free vortex sheet  $z_w(\Gamma, t)$  is determined by the circulation shedding rates  $\dot{\Gamma}_w$ , according to the Kutta condition, which states that the fluid velocity at the trailing edge is finite and tangent to the flyer. The Kutta condition can be obtained from the Euler equations by enforcing that, at the trailing edge, the difference in pressure across the swimmer is zero. To this end, we integrate the balance of momentum equation for inviscid planar flow along a closed contour containing the

vortex sheet and trailing edge,

$$[p]_{\mp}(s) = p_{-}(s) - p_{+}(s) = -\frac{d\Gamma(s, t)}{dt} - \frac{1}{2}(u_{-}^2 - u_{+}^2), \quad (\text{A } 6)$$

where  $\Gamma(s, t) = \Gamma_w + \int_{-l}^s \gamma(s', t) ds'$ ,  $-l \leq s \leq l$ , is the circulation within the contour and  $p_{\mp}(s, t)$  and  $u_{\mp}(s, t)$  denote the limiting pressure and tangential slip velocities on both sides of the swimmer. Since the pressure difference across the free sheet is zero, it also vanishes at the trailing edge by continuity, which implies that

$$\dot{\Gamma}_w = -\frac{1}{2}(u_{-}^2 - u_{+}^2)|_{s=-l}. \quad (\text{A } 7)$$

The values of  $u_{-}$  and  $u_{+}$  are obtained from the average tangential velocity component and from the velocity jump at the trailing edge, given by the sheet strength, evaluated at  $s = -l$

$$\bar{u} = \frac{u_{+} + u_{-}}{2} = \text{Im}[(w - w_{\text{swimmer}})n], \quad u_{-} - u_{+} = \gamma. \quad (\text{A } 8)$$

Once shed, the vorticity in the free sheet moves with the flow. Thus the parameter  $\Gamma$  assigned to each particle  $z_w(\Gamma, t)$  is the value of  $\Gamma_w$  at the instant it is shed from the trailing edge. The evolution of the free vortex sheet  $z_w$  is obtained by advecting it in time with the fluid velocity,

$$\dot{z}_w = w_w(z_w, t) + w_b(z_w, t). \quad (\text{A } 9)$$

## Appendix B. Forces and moments

The hydrodynamic force acting on the swimmer due to the pressure difference across the swimmer is given by,

$$\int_{l_b} n[p]_{\mp} ds = -F \sin \theta + iF \cos \theta, \quad (\text{B } 1)$$

where  $F = \int_{l_b} [p]_{\mp} ds$ . The hydrodynamic moment acting on the swimmer about its leading edge is given by

$$M = \text{Re} \left[ \int_{l_b} i \bar{n}(z_{le} - z_b) [p]_{\mp} ds \right], \quad (\text{B } 2)$$

where  $z_{le}$  is position of the leading edge  $s = \pm l$ .

It is known that the strength of the bound vortex sheet exhibits an inverse square root singularity at the edges (Saffman (1992); Eldredge (2019)). The singularity at the trailing edge is regularized by enforcing the Kutta condition as discussed above. To regularize the singularity at the leading edge, we introduce a force parallel to the plate known as leading edge suction (Eldredge 2019). Following the derivation provided in Eldredge (2019), we write the suction force, in dimensionless form as

$$S = 2\pi e^{i\theta} \sigma^2, \quad (\text{B } 3)$$

where  $\sigma$  is the suction parameter defined as

$$\sigma = \frac{1}{2}(\dot{y} - l\dot{\theta} \cos \theta) + \int_{l_b} \frac{\gamma(s, t)}{2\pi l} \text{Re} \left( \frac{\tilde{z}(s, t) + l}{\tilde{z}(s, t) - l} \right)^{1/2} ds \quad (\text{B } 4)$$

where  $\tilde{z}(s, t) = z(s, t) - ze^{i\theta}$ , is the complex position of any vortex sheet present in the fluid written in the plate's frame of reference.  $\dot{y} - l\dot{\theta} \cos \theta$  is the velocity of the center of

the plate in the  $y$ -direction. Note that in equation B 3, the suction force is always positive (always a thrust force) and parallel to the plate.

Note that the majority of the suction force is due to the vertical motion of the leading edge relative to the surrounding fluid. For the pitching swimmer, since the leading edge has no vertical motion, the contribution of the leading edge suction force to the total thrust force of the swimmer is negligible. This is confirmed by our numerical experiments on a single pitching swimmer.

Last, we introduce a drag force  $D$  that emulates the effect of skin friction due to fluid viscosity. This force is based on the Blasius laminar boundary layer theory as implemented by Fang (2016) in the context of the vortex sheet model. Blasius theory provides an empirical formula for skin friction on one side of a horizontal plate of length  $2l$  placed in fluid of density  $\rho_f$  and uniform velocity  $U$ . In dimensional form, Blasius formula is  $D = -\frac{1}{2}\rho_f(2l)(c_f)U^2$ , where the skin friction coefficient  $C_f = 0.664/\sqrt{\text{Re}}$  is given in terms of the Reynolds number  $\text{Re} = \rho_f U(2l)/\mu$ . Substituting back in the empirical formula leads to  $D = -C_d U^{3/2}$ , where  $C_d = 0.664\sqrt{\rho_f \mu(2l)}$ . Following Fang (2016), we write a modified expression of the drag force for a swimming plate

$$D = -C_d(\overline{U}_+^{3/2} + \overline{U}_-^{3/2}), \quad (\text{B } 5)$$

where  $\overline{U}_\pm$  are the spatially-averaged tangential fluid velocities on the upper and lower side of the plate, respectively, relative to the swimming velocity  $U$ ,

$$\overline{U}_\pm(t) = \frac{1}{2l} \int_{-l}^l u_\pm(s, t) ds - U. \quad (\text{B } 6)$$

We estimate  $C_d$  to be approximately 0.02 in the experiments of Ramananarivo *et al.* (2016).

## Appendix C. Numerical implementation

The bound vortex sheet is discretized by  $2n + 1$  point vortices at  $z^b(t)$  with strength  $\Delta\Gamma = \gamma\Delta s$ . These vortices are located at Chebyshev points that cluster at the two ends of the swimmer. Their strength is determined by enforcing no penetration at the midpoints between the vortices, together with conservation of circulation. The free vortex sheet is discretized by regularized point vortices at  $z^w(t)$ , that is released from the trailing edge at each timestep with circulation given by (A 7). The free point vortices move with the discretized fluid velocity while the bound vortices move with the swimmer's velocity. The discretization of equations (2.2) and (A 7, A 9) yields a coupled system of ordinary differential evolution equations for the swimmer's position, the shed circulation, and the free vorticity, that is integrated in time using the 4th order Runge-Kutta scheme. The details of the shedding algorithm are given in Nitsche & Krasny (1994). The numerical values of the timestep  $\Delta t$ , the number of bound vortices  $n$ , and the regularization parameter  $\delta$  are chosen so that the solution changes little under further refinement.

Finally, to emulate the effect of viscosity, we allow the shed vortex sheets to decay gradually by dissipating each incremental point vortex after a finite time  $T_{\text{diss}}$  from the time it is shed into the fluid. Larger  $T_{\text{diss}}$  implies that the vortices stay in the fluid for longer times, mimicking the effect of lower fluid viscosity. For the results depicted in this study, we used  $T_{\text{diss}} \in [1.5, 3.5]$  flapping period. We refer the reader to Huang *et al.* (2018) for a detailed analysis of the effect of dissipation time on the hydrodynamic forces on a stationary and moving plate in the vortex sheet model. Details of the numerical

validation in comparison to Jones (2003) and Jones (2005) are provided in Huang *et al.* (2016).

## Appendix D. Swimming Energetics

Heaving motions are produced by an active heaving force  $F_h$  acting by the swimmer on the fluid in the  $y$ -direction. The value of  $F_h$  is obtained from the balance of linear momentum on the swimmer in the  $y$ -direction,

$$\text{Heaving: } m\ddot{y} = F_y + F_h. \quad (\text{D } 1)$$

Here, the hydrodynamic force  $F_y$  acting on the swimmer in the  $y$ -direction is given by (B 1).

Pitching motions are produced by an active moment  $M_p$  acting by the swimmer on the fluid about the leading edge. The value of  $M_p$  is obtained from the balance of angular momentum about the swimmer's leading edge,

$$\text{Pitching: } I\ddot{\theta} - \text{Im}[m(\dot{x} + i\dot{y})w_{\text{l.e.}}] = M + M_p, \quad (\text{D } 2)$$

Here,  $I = m(2l)^2/3$  is the swimmer's moment of inertia about the leading edge,  $w_{\text{l.e.}}$  is the swimmer's velocity at the leading edge, and  $M$  is the hydrodynamic moment about the leading edge given in (B 2).

The power input by the swimmer into the fluid due to heaving and pitching motions, respectively, is given by

$$\begin{aligned} \text{Heaving: } P_h &= F_h \dot{y}, \\ \text{Pitching: } P_p &= M_p \dot{\theta}. \end{aligned} \quad (\text{D } 3)$$

Note that in both cases, the leading edge suction and skin drag forces do not contribute to the input power.